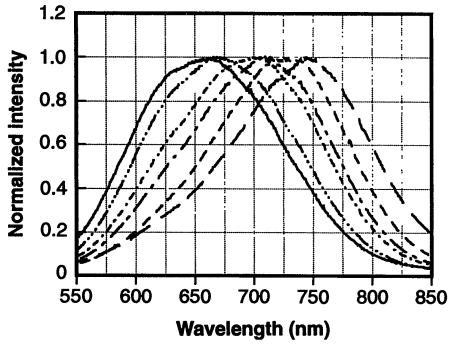

Fig. 3. Photoemission spectra from various spots on the etched image. The spectra were obtained with an expanded He/Cd laser (442 nm, ~0.5 mW cm^{-2}) excitation source and a Princeton Instruments charge-coupled device photodetector/Acton Research 0.25-m monochromator fitted with a fiber optic and microscope objective lens to allow detection from small (<1 mm^2) sample areas.

more brightly illuminated during the photoelectrochemical etch. The same variations were seen on wafers with porous Si layers that were too thick to display the optical interference phenomena.

Thus, the shift in wavelength maximum (λ_{max}) can be attributed to variations in the inherent emissive properties of the porous Si. The PL emission maximum on porous Si depends on the etch rate used in the electrochemical etch (*14*). Because the photocurrent at *n*-Si is proportional to light intensity (*15*), the intensity variation across the projected image translates into a variation in the etch rate, which presumably leads to the different emission maxima observed. The correlation of the PL λ_{max} to photoetch light intensity was confirmed in separate measurements with the use of uniform photoetch illumination. The value of λ_{max} ranged from 710 to 640 nm for photoetch light intensities ranging from 3×10^{14} to 12×10^{14} photon cm^{-2} s^{-1}. The emission maxima were also sensitive to the etch duration and current densities used. In our experiments, the etching time was 30 min at a current density of 100 μA cm^{-2}.

The background in the picture that we used included a grid pattern. At the reduction ratios used, the replica of the grid produced on the *n*-Si substrate contained 20 lines per millimeter in each direction. Illumination of this area with a He/Ne laser generated a diffraction pattern. The spot spacing matched that predicted from the grating equation for Fraunhofer diffraction (*16*) and corresponded to a line separation on the *n*-Si substrate of 50 μm. Profilometry measurements (Dektak 3030) showed no height modulation (less than ±20 nm) on the porous Si layer, which indicates that the surface of the etched grating was relatively flat. Because the porosity of anodized porous Si depends on etch current density (*17, 18*), the observed diffraction presumably resulted from a periodic density (and refractive index) variation within the etched wafer. This morphology differs from that of conventional ruled gratings, which consist of mechanically imprinted grooves on a surface.

REFERENCES AND NOTES

1. L. T. Canham, *Appl. Phys. Lett.* **57**, 1046 (1990).
2. V. Lehmann and U. Gosele, *ibid.* **58**, 856 (1991).
3. A. G. Cullis and L. T. Canham, *Nature* **353**, 335 (1991).
4. A. Bsiesy *et al.*, *Surf. Sci.* **254**, 195 (1991).
5. L. T. Canham, M. R. Houlton, W. Y. Leong, C. Pickering, J. M. Keen, *J. Appl. Phys.* **70**, 422 (1991).
6. S. M. Prokes, O. J. Glembocki, V. M. Bermudez, R. Kaplan, paper presented at the fall meeting of the Materials Research Society, Boston, MA, 2–6 December 1991.
7. Y. H. Xie, W. L. Wilson, F. M. Ross, J. A. Mucha, E. A. Fitzgerald, paper presented at the fall meeting of the Materials Research Society, Boston, MA, 2–6 December 1991.
8. M. S. Brandt, H. D. Fuchs, M. Stutzmann, J. Weber, M. Cardona, *Solid State Commun.* **81**, 307 (1992).
9. R. P. Vasquez, R. W. Fathauer, T. George, A. Ksendzov, T. L. Lin, *Appl. Phys. Lett.* **60**, 1004 (1992).
10. V. V. Doan and M. J. Sailor, *ibid.*, p. 619.
11. Several methods that take advantage of semiconductor photochemistry or photoelectrochemistry have been devised to generate either permanent or temporary images at a semiconductor surface (*19–24*).
12. E. Hecht, *Optics* (Addison-Wesley, Reading, MA, 1987), pp. 333–378.
13. K. L. Chopra and I. Kaur, *Thin Film Device Applications* (Plenum, New York, 1983), pp. 55–58.
14. N. Koshida and H. Koyama, *Jpn. J. Appl. Phys.* **30**, L1221 (1991).
15. N. S. Lewis, *J. Electrochem. Soc.* **131**, 2496 (1984).
16. M. Born and E. Wolf, *Principles of Optics* (Pergamon, Oxford, 1970), pp. 401–411.
17. G. Bomchil, A. Halimaoui, R. Herino, *Appl. Surf. Sci.* **41–42**, 604 (1989).
18. R. Herino, G. Bomchil, K. Barla, C. Bertrand, J. L. Ginoux, *J. Electrochem. Soc.* **134**, 1994 (1987).
19. R. M. Osgood, A. Sanchez-Rubio, D. J. Ehrlich, V. Daneu, *Appl. Phys. Lett.* **40**, 391 (1982).
20. T. Inoue, A. Fujishima, K. Honda, *J. Electrochem. Soc.* **127**, 1582 (1980).
21. R. H. Micheels, A. D. Darrow, R. D. Rauh, *Appl. Phys. Lett.* **39**, 418 (1981).
22. R. D. Rauh and R. A. LeLievre, *J. Electrochem. Soc.* **132**, 2811 (1985).
23. T. L. Rose, D. H. Longendorfer, R. D. Rauh, *Appl. Phys. Lett.* **42**, 193 (1983).
24. J. D. Venables and R. M. Broudy, *J. Appl. Phys.* **30**, 1110 (1959).

5 March 1992; accepted 8 May 1992

Energetics of Large Fullerenes: Balls, Tubes, and Capsules

Gary B. Adams, Otto F. Sankey,* John B. Page, Michael O'Keeffe, David A. Drabold

First-principles calculations were performed to compare the energies of 29 different fullerene structures, with mass number from 60 to 240, and of eight nonhelical graphite tubes of different radii. A quantity called the planarity, which indicates the completeness of the π-bonding, is the single most important parameter determining the energetics of these structures. Empirical equations were constructed for the energies of nonhelical tubes and for those fullerene structures that may be described as balls or capsules. For a given mass number, ball-shaped fullerenes are energetically favored over capsular (tube-like) fullerenes.

The discovery and practical synthesis (*1, 2*) of C_{60} has prompted the search for other fullerene-like molecules and other novel forms of carbon. Lamb *et al.* (*3*) have created samples containing a wide variety of large carbon fullerenes of mass number up to 290. Scanning tunneling microscope images have shown that the molecules in these samples are exclusively ball-shaped. Graphitic tubes (*4, 5*) and fullerene capsules (*6*) are other forms that have been proposed and imaged. At present, there are no simple yet reliable estimates for the energies of these various structures.

In this report we present computations of the equilibrium configurations and compare the energies of three different types of carbon structures: fullerene balls, graphitic tubes, and fullerene capsules (a tube with ball-like caps). In these computations we used quantum molecular dynamics (QMD) (*7–9*) simulations. Thirty-seven different structures were simulated, and from these ab initio results we created simple empirical formulas for predicting the energy of any size fullerene ball, tube, or capsule. These empirical formulas are based on only one parameter, the "planarity," which is defined from the π-bonding angle (π angle, or ϕ_π). The energetic effect of the size of the HOMO-LUMO gap (highest occupied and lowest unoccupied molecular orbitals) was found to be of secondary importance. For a fixed number of atoms, fullerene balls are

G. B. Adams, O. F. Sankey, J. B. Page, Department of Physics and Astronomy, Arizona State University, Tempe, AZ 85287.
M. O'Keeffe, Department of Chemistry, Arizona State University, Tempe, AZ 85287
D. A. Drabold, Department of Materials Science and Engineering, University of Illinois, Urbana, IL 61801.
*To whom correspondence should be addressed.

energetically preferred over long, tube-like capsules.

Iijima has imaged helical tubes of graphitic carbon (*4*), using an electron microscope. Although the effect of the helical pitch on the energetics is not yet known, we do not expect it to be the predominant energy contribution. Instead, it is expected to be an aid in the growth of the tubes. We consider here the two types of nonhelical graphitic tubes, $T_\perp$ and $T_\parallel$ (Fig. 1). A helical tube would be, geometrically at least, in between these two limits.

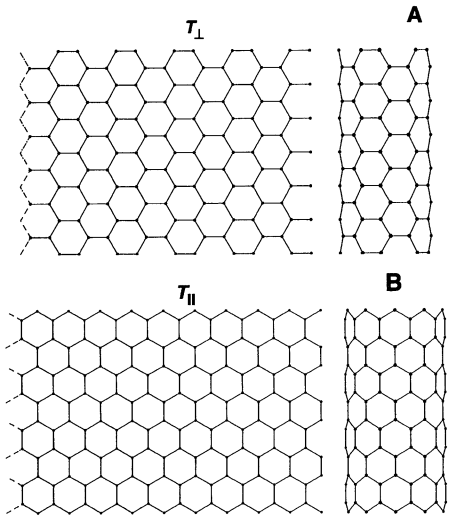

Fig. 1. (**A**) On the right is shown a segment of an infinite $T_\perp$ ($n_\perp$ = 10) graphitic tube. On the left the same segment is unrolled into a flat graphitic sheet. (**B**) On the right is shown a segment of an infinite $T_\parallel$ ($n_\parallel$ = 20) graphitic tube. On the left the same segment is unrolled into a flat graphitic sheet.

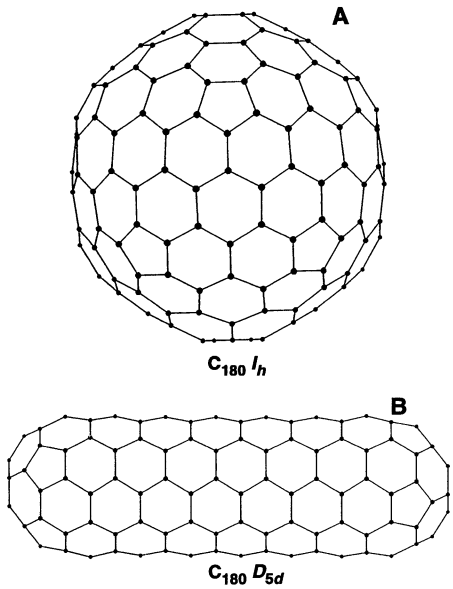

Fig. 2. (**A**) The ball-like fullerene I_h C_{180}. (**B**) The capsular fullerene D_{5d} C_{180}, the longest and thinnest of the C_{180} capsules considered here.

We computed the equilibrium energies of $T_\perp$ and $T_\parallel$ tubes of infinite length and varying numbers of carbon atoms around the circumference ($n_\perp$ and $n_\parallel$, respectively), using QMD. The periodicity along the tube was fixed at a value appropriate for a bond length d of single-plane graphite (1.42 Å). The radius of the tube was free to adjust during the QMD relaxation. The computed total energies per atom (relative to that of single-plane graphite) for various numbers of carbon atoms around the circumference are shown in Table 1.

We can model the computed energies of graphitic tubes with a single variable, the planarity of the tube. In a tight-binding model, the interaction between two nearly parallel neighboring π orbitals is proportional to $\cos(\phi_\pi)$. We define the planarity of a structure to be the average value of $\cos(\phi_\pi)$ for that structure. We take the normal of the tube to define the direction of the π orbital at each atom so that $\phi_\pi \approx d_\perp/r$, where $d_\perp$ is the distance between the two neighboring atoms in a direction perpendicular to the tube axis and r is the tube radius. The energy per atom of the tube with respect to planar graphite is then modeled as

$$E_{\perp(\parallel)}(\phi_\pi) = k_{\perp(\parallel)}[1 - \cos(\phi_\pi)] \quad (1)$$

where only one parameter ($k_\perp$ or $k_\parallel$) is needed for each type of tube. We average $\cos(\phi_\pi)$ over three neighboring atoms in $T_\perp$ and $T_\parallel$ tubes to give

$$\phi_\pi(T_\perp) = \cos^{-1}\left[\frac{2\cos\left(\frac{d}{2r}\right) + \cos\left(\frac{d}{r}\right)}{3}\right] \quad (2a)$$

$$\phi_\pi(T_\parallel) = \cos^{-1}\left[\frac{2\cos\left(\frac{\sqrt{3}d}{2r}\right) + 1}{3}\right] \quad (2b)$$

For large r, these become

$$\phi_\pi \approx \frac{\sqrt{2}d}{2r} \quad (3)$$

for both $T_\perp$ and $T_\parallel$ tubes. The parameter $k_\perp$ is fit to our QMD result at $n_\perp$ = 10, and $k_\parallel$ is fit at the QMD result at $n_\parallel$ = 18. The values of k so found are $k_\perp$ = 4.195 eV and $k_\parallel$ = 4.150 eV. We show in Table 1 the π-angle ϕ_π and the energy as determined from our empirical energy formula (Eq. 1); the QMD and empirical formulas agree very well. Since $r \propto n_{\perp(\parallel)}$, and $\phi_\pi \propto 1/r$, the energy of a tube for large $n_{\perp(\parallel)}$ is $E_{\perp(\parallel)}(n) \approx \frac{1}{2} k_{\perp(\parallel)}\phi_\pi^2 \propto 1/n_{\perp(\parallel)}^2$.

Next we model large fullerenes (*3*) and assume that they all have 12 isolated five-membered rings and [(*n*/2) − 10] six-membered rings. The QMD-relaxed molecules that are most nearly spherical are the icosahedral molecules I_h C_{60}, I_h C_{80}, I C_{140}, I_h C_{180} (Fig. 2A), and I_h C_{240}. We have not compared I_h C_{240} with other structural models, but both I C_{140} and I_h C_{180} were lower in energy than all other simulated structures of the same mass. We find that I_h C_{80} is the only one of the simulated "spherical" fullerenes that is higher in energy than a less spherical structure, in this case D_{5d} C_{80}, one of the capsular fullerenes discussed below. Our computed total energies per atom for all of these ball-like structures are listed in Table 2.

For spherical surfaces of radius r, $\phi_\pi \approx d/r$, where d is the spacing (bond length) between adjacent atoms on the surface. Thus r is determined by the number of atoms n and the surface number density $\sigma = (n/4\pi r^2)$, which we assume to be approximately constant for fullerene balls, so that $r \propto \sqrt{n}$. Furthermore, if d is approximately a constant, we have

$$\phi_\pi(n) \approx \phi_\pi(60)\sqrt{60/n} \quad (4)$$

where $\phi_\pi(60)$ is the π angle for relaxed I_h C_{60} (23.14°).

We model the total energy of a large fullerene ball by separating the molecules into their "pentagon" atoms and their "hexagon" atoms. By hexagon atoms, we mean atoms surrounded on all sides by six-membered

Table 1. The QMD and approximate energies per atom (relative to that of single-plane graphite) of $T_\perp$- and $T_\parallel$-type graphitic tubes of radius r. The number of atoms around the circumference is $n_\perp$ ($n_\parallel$) and the average π angle is ϕ_π.

$n_{\perp,\parallel}$	$r_{\perp,\parallel}$ (Å)	E (QMD) (eV/atom)	ϕ_π		E (approx.) (Eq. 1)
		$T_\perp$ *infinite tubes*			
10	3.39	0.182	16.94°		0.182 (fit)
12	4.07	0.126	14.12°		0.127
16	5.43	0.071	10.59°	Eq. 2a	0.071
20	6.78	0.045	8.48°		0.046
		$T_\parallel$ *infinite tubes*			
18	3.52	0.167	16.32°		0.167 (fit)
20	3.91	0.133	14.69°		0.136
24	4.69	0.094	12.25°	Eq. 2b	0.094
30	5.87	0.060	9.79°		0.060

rings. In I_h C_{60}, all atoms are pentagon atoms, because there are no atoms entirely surrounded by six-membered rings. The total energy is modeled as

$$E(\phi_\pi) = \frac{(n - 60)k(1 - \cos\phi_\pi) + 60E_{60}}{n} \quad (5)$$

where E_{60} is the energy per atom for I_h C_{60}. For the hexagon atoms, we apply the same $(1 - \cos\phi_\pi)$ factor as for graphitic tubes. However, the five-membered rings in an icosahedral molecule are always located at the vertices of the icosahedron onto which the molecule may be mapped, and the sum of the angles surrounding the pentagon atoms is always about 120° + 120° + 108° = 348°, implying that ϕ_π for the pentagon atoms changes very little as the molecule gets larger. Therefore, no $(1 - \cos\phi_\pi)$ factor is included for pentagon atoms. Fitting k is done to the energy of I_h C_{240} and yields k = 3.18 eV. The energy dependence on ball size n for large balls can be seen from Eq. 5. Because ϕ_π scales as $1/\sqrt{n}$ from Eq. 4, for large n (small ϕ_π) Eq. 5 becomes

$$E(n) = \left[E_{60} + \frac{1}{2}k\phi_\pi^2(60)\right]\left(\frac{60}{n}\right) - \frac{1}{2}k\phi_\pi^2(60)\left(\frac{60}{n}\right)^2 = 0.6976\left(\frac{60}{n}\right) - 0.2593\left(\frac{60}{n}\right)^2 \text{ eV/atom} \quad (6)$$

The energies of I C_{140} and I_h C_{180} are well reproduced by our simple formula (Eq. 5) (Table 2). Surprisingly, the formula is also quite successful at reproducing the energies of the lowest energy fullerenes having other numbers of atoms. For C_{120} fullerenes, for example, the simulated molecule with the lowest energy is the T_d form. The QMD energy of T_d C_{120} is about 0.002 eV per atom less than the value produced by our simple model. For C_{84}, the simulated fullerene with the lowest energy is the D_{6h} form, the energy of which is 0.008 eV per atom less than the value produced by the model. In view of these results, we regard Eq. 5, derived empirically from our results for icosahedral balls, as approximately representing the minimum energy (to within about 0.01 eV per atom) for any large fullerene structure of a given mass. This energy minimum may not always be obtainable but should be approached, for a given n, as the planarity of the n-atom molecule approaches the planarity of an n-atom sphere.

Finally, we consider capsules, which are graphitic tubes with more or less hemispherical caps of carbon atoms on each end (such as D_{5d} C_{180}, Fig. 2B). We first present a simple argument showing that, if one considers planarity only, fullerene balls should be energetically favored over capsules. Then we present our QMD results, which verify this prediction.

For both balls and tubes, our empirical formulas show that the energy per atom of the structure monotonically decreases as the average π angle decreases. We consider capsules, which have a tube of length z and radius ρ capped by hemispheres of radius ρ. We then ask, for a given surface area σ of a capsule, what length z minimizes ϕ_π^2? The surface area σ is $2\pi z\rho + 4\pi\rho^2$. The π angle of the hemisphere is d/ρ, while that of the tube (Eq. 3) is $\sqrt{2}d/2\rho$. The average ϕ_π^2 is then

$$\overline{\phi_\pi^2} = \frac{\frac{1}{2}\sigma_{\text{tube}} + \sigma_{\text{caps}}}{\sigma}(d/\rho)^2 = \frac{(z/\rho) + 4}{\sigma}\pi d^2 \quad (7)$$

which is clearly a minimum when $z/\rho = 0$.

With our QMD program, we have simulated four types of fullerene capsules: two types with fivefold symmetry and two types with sixfold symmetry (*10*). The energies

Table 2. The QMD and approximate energies per atom (relative to that of single-plane graphite) of fullerene ball-like molecules and the average π angle of the molecule assuming a perfect sphere.

Fullerene	Symmetry	E (QMD) (eV/atom)	ϕ_π (Eq. 4)	E (approx.) (Eq. 5)
C_{60}	I_h	0.4383	23.14°	0.438 (fit)
C_{80}	I_h	0.3870	20.04°	0.376
C_{80}	D_{5h}	0.3780	20.04°	0.376
C_{84}	T_d	0.3685	15.96°	0.365
C_{84}	D_2 (*11*)	0.3594	15.96°	0.365
C_{84}	D_{6h}	0.3570	15.96°	0.365
C_{120}	D_{6d}	0.2892	16.36°	0.284
C_{120}	D_6	0.2881	16.36°	0.284
C_{120}	T_d	0.2818	16.36°	0.284
C_{140}	I	0.2452	15.15°	0.251
C_{180}	$D_{5'}$	0.2031	13.36°	0.203
C_{180}	I_h	0.2006	13.36°	0.203
C_{240}	I_h	0.1580	11.57°	0.158 (fit)

Table 3. The QMD and approximate energies per atom (relative to that of single-plane graphite) of a sequence of capsules with caps made from "spherical" forms of C_{60}, C_{80}, C_{84}, and C_{120}. These capsules have either $T_\perp$-type or $T_\parallel$-type tubes containing belts of $n_\perp$ or $n_\parallel$ atoms around the circumference.

Capsule	Symmetry	No. of added belts	E (QMD) (eV/atom)	E (approx.) (Eq. 8)
		Capsules with C_{60} caps ($n_\perp$ = 10)		
C_{60}	I_h	0	0.4383	0.438
C_{70}	D_{5h}	1	0.3948	0.402
C_{80}	D_{5d}	2	0.3770	0.374
C_{120}	D_{5d}	6	0.3088	0.310
C_{130}	D_{5h}	7	0.2980	0.300
C_{140}	D_{5d}	8	0.2917	0.292
C_{180}	D_{5d}	12	0.2669	0.267
		Capsules with C_{80} caps ($n_\parallel$ = 20)		
C_{80}	I_h	0	0.3870	0.387
C_{120}	$D_{5d'}$	2	0.3040	0.302
C_{120}	D_{5h}	2	0.3001	0.302
C_{140}	D_5	3	0.2783	0.278
C_{180}	D_5	5	0.2466	0.246
		Capsules with C_{84} caps ($n_\perp$ = 12)		
C_{84}	D_{6h}	0	0.3570	0.357
C_{96}	D_{6d}	1	0.3299	0.328
C_{120}	D_{6d}	3	0.2892	0.288
C_{180}	D_{6h}	8	0.2350	0.234
C_{228}	D_{6h}	12	0.2121	0.211
		Capsules with C_{120} caps ($n_\parallel$ = 24)		
C_{120}	D_6	0	0.2881	0.288
C_{144}	D_{6d}	1	0.2649	0.256
C_{144}	D_{6h}	1	0.2581	0.256

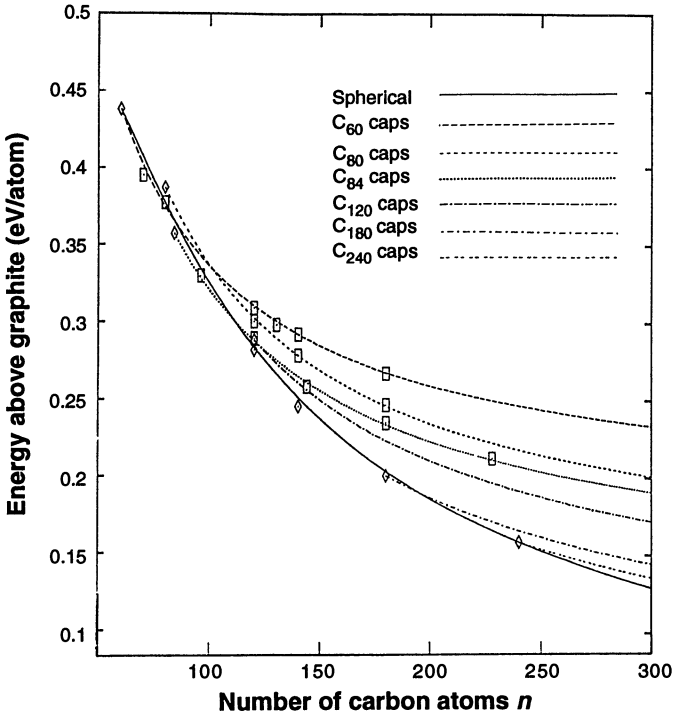

Fig. 3. The energies per atom (relative to that of single-plane graphite) of a selection of simulated fullerenes plotted against the mass numbers of those fullerenes. The energies of ball-like fullerenes (from Table 2) are given by diamonds. In each case, except for C_{80}, the energy of the selected ball-like fullerene is the lowest energy attained for that mass number. (For C_{120}, the two lowest energies are plotted.) The energies of capsular fullerenes (from Table 3) are given by rectangles. The broken curves are plots of capsular empirical equations derived by substitution into Eq. 8. The solid curve is a plot of Eq. 5 for ball-like fullerenes. Each of the broken curves originates from a diamond on or near the solid curve, but the broken curves diverge from the solid curve as n increases.

per atom computed for the relaxed configurations of these fullerene capsules are listed in Table 3. Comparing Tables 2 and 3, one sees that capsules of a given mass number are higher in energy than ball-like fullerenes of the same mass number. Also, longer thinner capsules of a given mass are higher in energy than shorter fatter capsules of the same mass. The one exception to these rules is for the energy of I_h C_{80} as compared to D_{5d} C_{80}.

The energy of a capsule can be modeled as the energy of the "spherical" cap plus the energy of the finite tube

$$E_{\text{capsule}}(n) = \frac{(n - n_{\text{cap}})E_{\text{tube}} + n_{\text{cap}}E_{\text{cap}}}{n} \quad (8)$$

Here E_{capsule}, E_{tube}, and E_{cap} are, respectively, the energies per atom relative to that of single-plane graphite for the capsule, the tube that forms the length of the capsule, and the "spherical" fullerene that is separated to form the caps. The number of atoms contained in the caps is n_{cap}, and n is the total number of atoms in the capsule. Energies computed from Eq. 8 are given in Table 3.

We now summarize our results by plotting in Fig. 3 the energy per atom of ball-like fullerenes and fullerene capsules for various numbers of atoms n. For icosahedral fullerenes, the only significant deviation of the QMD results from the empirical formula is for I_h C_{80}. The solid line in Fig. 3 (Eq. 5) represents an approximate energy minimum line for fullerene structures, which may not always be obtainable.

The broken curves in Fig. 3 correspond to capsules. Six sequences of capsules are shown, having caps made from "spherical" forms of C_{60}, C_{80}, C_{84}, C_{120}, C_{180}, and C_{240}. These curves correspond to the simplified formula of Eq. 8. The QMD results for the capsules with caps made from C_{60}, C_{80}, C_{84}, and C_{120} are given by the rectangles in Fig. 3. The asymptote for each capsule curve is the energy of the graphitic tube from which that capsule can be constructed (see Tables 1 and 3). The energies of the capsules with caps made from C_{60}, C_{80}, C_{84}, C_{120}, C_{180}, and C_{240} asymptotically approach the $n_\perp = 10, n_\parallel = 20, n_\perp = 12, n_\parallel = 24, n_\parallel = 30$, and $n_\perp = 20$ infinite tube energies, respectively.

The most important conclusion from Fig. 3 is that, for a given number of atoms, long fullerene capsules are much higher in energy than spherical fullerenes. For example, a C_{180} capsule is far higher in energy (per atom) than a C_{180} icosahedral fullerene. This suggests that the process of Lamb *et al.* (3) for obtaining higher fullerenes, which shows no signs of tubular structures, is synthesizing only the lowest energy fullerenes for each mass number. The calculations presented here do not rule out the existence of capsules because they give only the energetics of the structures and do not include the kinetics of the formation process.

REFERENCES AND NOTES

1. H. W. Kroto, J. R. Heath, S. C. O'Brien, R. E. Curl, R. E. Smalley, *Nature* **318**, 162 (1985).
2. W. Kratschmer, L. D. Lamb, K. Fostiropoulos, D. R. Huffman, *ibid.* **347**, 354 (1990).
3. L. D. Lamb *et al.*, *Science* **255**, 1413 (1992).
4. S. Iijima, *Nature* **354**, 56 (1991).
5. J. W. Mintmire, B. I. Dunlap, C. T. White, *Phys. Rev. Lett.* **68**, 631 (1991).
6. S. Wang and P. R. Buseck, *Chem. Phys. Lett.* **182**, 1 (1991).
7. We used an ab initio QMD technique in the local density approximation with norm-conserving pseudopotentials within a localized sp^3 pseudoatomic orbital basis. The approximate density functional we use is due to J. Harris [*Phys. Rev. B* **31**, 1770 (1985)]. The method has been thoroughly tested, and the details are described in previous work (*8, 9*). At each time step, the electronic states are calculated for the instantaneous atomic configuration, and from these electronic states the forces on each atom are determined. The atoms then are moved according to Newton's laws. The method has a number of approximations that make it computationally very fast, and it is ideally suited for studying large fullerenes. There are no adjustable parameters. In the work reported here, we use the QMD method to geometrically relax approximate initial structures by imposing an artificial damping that causes the atoms to settle into an equilibrium configuration. At this final time step (as in all steps) we obtain charge densities, molecular orbitals, forces, and total energies.
8. O. F. Sankey and D. J. Niklewski, *Phys. Rev. B* **40**, 3979 (1989).
9. G. B. Adams *et al.*, *ibid.* **44**, 4052 (1991).
10. The two types of fivefold capsules are $T_\perp$ ($n_\perp$ = 10) tubes with I_h C_{60} caps and $T_\parallel$ ($n_\parallel$ = 20) tubes with I_h C_{80} caps. In each case the caps are polar hemispheres of the icosahedral molecules oriented so that five-membered rings are centered at the poles. The simulated capsules with C_{60} caps are D_{5h} C_{70}, D_{5d} C_{80}, D_{5d} C_{120}, D_{5h} C_{130}, D_{5d} C_{140}, and D_{5d} C_{180}. The simulated capsules with C_{80} are D_{5d} C_{120}, D_{5h} C_{120}, D_5 C_{140}, and D_5 C_{180}. The two types of simulated capsules with sixfold symmetry are made of $T_\perp$ ($n_\perp$ = 12) tubes and $T_\parallel$ ($n_\parallel$ = 24) tubes. The caps of the $T_\perp$ ($n_\perp$ = 12) tubes are halves of the D_{6d} C_{72} molecule; however, these 36-atom halves are quite flattened and are far from hemispherical. The first tube in the sequence is D_{6h} C_{84}, which is much more spherical than D_{6d} C_{72}. For this reason we refer to the caps of these capsules as C_{84} caps, even though one of the "halves" already has an $n_\perp$ = 12 belt attached to it. The simulated capsules with C_{84} caps are D_{6h} C_{84}, D_{6d} C_{96}, D_{6d} C_{120}, D_{6d} C_{180}, and D_{6h} C_{228}. Similarly, we refer to the caps of the $T_\parallel$, ($n_\parallel$ = 24) tubes as C_{120} caps even though they are really two D_{6h} C_{96} halves, one of which has a single $n_\parallel$ = 24 belt attached to it. The simulated capsules with C_{120} caps are D_6 C_{120}, D_{6d} C_{144}, and D_{6h} C_{144}.
11. Achiba, unpublished data; S. Saito, S. Sawada, N. Hamada, in preparation.

12. Supported by the Office of Naval Research (ONR N00014-90-J-1304) and the National Science Foundation (DMR-9012143). J.B.P. acknowledges the support of the Alexander von Humboldt Foundation and the Institute for Theoretical Physics, University of Regensburg, Germany, during a portion of this research. We also appreciate stimulating conversations with L. D. Lamb, D. Sarid, S. Wang, P. R. Buseck, K. Sinha, and J. Menendez.

11 March 1992; accepted 5 May 1992